2018-8

Electrochemical Glucose Sensors Enhanced by Methyl Viologen and Vertically Aligned Carbon Nanotube Channels

Benjamin J. Brownlee

Meisam Bahari

John H. Harb

Jonathan C. Claussen

Brian D. Iverson
Brigham Young University - Provo, bdiverson@byu.edu

Original Publication Citation

Brownlee, B. J., Bahari, M., Harb, J. N., Claussen, J. C., and Iverson, B. D., 2018, "Electrochemical glucose sensors enhanced by methyl viologen and vertically aligned carbon nanotube channels," ACS Applied Materials & Interfaces (in press) DOI: 10.1021/acsami.8b08997

Electrochemical Glucose Sensors Enhanced by Methyl Viologen and Vertically Aligned Carbon Nanotube Channels

Benjamin J. Brownlee,[1] Meisam Bahari,[2] John N. Harb,[2]
Jonathan C. Claussen,[3] Brian D. Iverson[1]*

1 Department of Mechanical Engineering, Brigham Young University, Provo, UT, 84602
2 Department of Chemical Engineering, Brigham Young University, Provo, UT, 84602
3 Department of Mechanical Engineering, Iowa State University, Ames, IA, 50011

*Corresponding author email: bdiverson@byu.edu

Abstract

Free-standing, vertically aligned carbon nanotubes (VACNTs) were patterned into 16 μm diameter microchannel arrays for flow-through electrochemical glucose sensing. Non-enzymatic sensing of glucose was achieved by the chemical reaction of glucose with methyl viologen (MV) at an elevated temperature and pH (0.1 M NaOH), followed by the electrochemical reaction of reduced-MV with the VACNT surface. The MV sensor required no functionalization (including no metal) and was able to produce on average 3.4 electrons per glucose molecule. The current density of the MV sensor was linear with both flow rate and glucose concentration. Challenges with interference chemicals were mitigated by operating at a low potential of -0.2 V vs. Ag/AgCl. As a comparison, enzymatic VACNT sensors with platinum nano-urchins were functionalized with glucose oxidase by covalent binding (EDC/NHS) or by polymer entrapment (PEDOT) and operated in phosphate buffered saline (PBS). With normalization by the overall cross-sectional area of the flow (0.713 cm^2), the sensitivity of the MV, enzyme-in-solution, and covalent sensors were 45.93, 18.77, and 1.815 mA cm^{-2} mM^{-1}, respectively. Corresponding limits of detection were 100, 194, and 311 nM glucose. The linear sensing ranges for the sensors were: 250 nM – 200 μM glucose for the MV sensor, 500 nM – 200 μM glucose for the enzyme-in-solution sensor, and 1 μM – 6 mM glucose for the covalent sensor. The flow cell and sensor cross-sectional area were scaled down (0.020 cm^2) to enable detection from 200 μL of glucose with MV by flow injection analysis (FIA). The sensitivity of the small MV sensor was 5.002 mA cm^{-2} mM^{-1}, with a limit of detection of 360 nM glucose and a linear range up to at least 150 μM glucose. The small MV sensor has the potential to measure glucose levels found in 200 μL of saliva.

Keywords: electrochemical sensor, glucose, methyl viologen, vertically aligned carbon nanotubes (VACNTs), microchannel, flow injection analysis (FIA)

1. Introduction

With recent advances in nanomaterials, many glucose sensors have been able to greatly lower their detection limits. Metal and metal oxide nanoparticles,[1] along with carbon nanomaterials such as carbon nanotubes (CNTs),[2-4] graphene,[5-7] and graphene oxide[8] have been shown to be effective at increasing sensor sensitivity.[9] CNTs are favorable for electrochemical sensing because of their high surface area, mechanical strength and electrical conductivity.[10] Many sensors incorporate randomly dispersed nanomaterials (including CNTs) that are cast on an electrode surface.[11] This often requires the use of binders resulting in densely packed nanostructures with poor mechanical stability.[12] Nanostructures grown from an electrode surface, such as nanorods, have been shown to have greater stability, while allowing for greater exposed surface area.[13] In a similar fashion, vertically aligned carbon nanotubes (VACNTs) provide an ordered, preferential orientation of CNTs with high surface area to volume ratio enabling high sensitivity. Glucose sensors are often electrochemically based, which offers good repeatability, affordability, and ease of use as concentration levels can be quantified even in turbid solutions with a digital output.[14]

An additional means of improving sensitivity involves taking advantage of convection. Flow-through sensors improve the reaction-diffusion kinetics and consequently are more efficient at reacting the target analyte at the electrode surface than traditional bulk sensors. Highly efficient detection of hydrogen peroxide (H_2O_2) with a flow-through VACNT electrode has been demonstrated in convective environments,[15] but an investigation into the effectiveness of flow-through sensing for more complex analyte such as glucose is still needed. Flow-through sensors also have the potential for flow injection analysis (FIA), which enables use of much smaller sample volumes.[16]

When glucose is not broken down by the body efficiently, the levels of glucose in the blood stream rise, with the potential for diabetes mellitus as a common resulting metabolic disorder.[17] Over 400 million people have diabetes worldwide,[18] with many health risks involved if diabetes is not properly diagnosed and treated.[19] Thus, early and accessible diagnostics are important in reducing the negative side-effects of untreated diabetes. There has been much investigation in continuous glucose monitoring sensors[20] and non-intrusive methods as alternatives to traditional blood-pricking methods.[21] Saliva is a more accessible bodily fluid and studies have shown that glucose levels in saliva can be directly correlated to the glucose levels in blood.[22] However, the

glucose concentration in saliva is significantly lower than that of blood, requiring a more sensitive glucose sensor to measure glucose levels accurately.

Glucose has also been investigated as a clean alternative energy source through biofuel cells, with recent advances focusing on improving performance with nanomaterials.[23] Glucose-based biofuel cells are typically small-scale energy production devices and have been considered for applications such as self-powered medical devices.[24-25] While fuel cells typically have electrolyte flowing between two electrodes, it has also been shown that glucose biofuel cells can operate in flow-through conditions, with solution flowing through an entire biofuel cell.[26]

Both glucose sensors and biofuel cells commonly use the enzyme glucose oxidase (GOx) to react with glucose. Biofuel cells typically use an electron-mediator, while glucose sensors often convert glucose into H_2O_2, which in turn reacts electrochemically at the electrode surface. Enzymatic glucose sensors are often functionalized with GOx on the surface, and it has been shown that the functionalization technique greatly impacts the sensitivity, selectivity and longevity of such sensors.[27] Primary methods of electrode functionalization include: physical absorption, cross-linking, covalent bonding, bioaffinity bonding, and polymer entrapment. All enzymatic sensors are prone to enzyme detachment from the surface and to loss of enzyme activity over time; however, enzyme entrapment in conductive polymers has shown to be an effective method of functionalizing the glucose oxidase to maintain stability and functional form with minimal adverse steric effects.[28] Shi, et al. have provided a comparison of functionalization methods for sol-gel encapsulation and glutaraldehyde cross-linking,[29] but there lacks a comparison between different functionalization methods for high-aspect-ratio microstructures, where the functionalization needs to penetrate far beyond the easily accessible outer surface.

In recent literature there has been a trend in the development of non-enzymatic glucose sensors.[30] Non-enzymatic sensors have risen in popularity due to their ease of manufacturing and because they do not have the same stability concerns common to enzymatic sensors.[31] Moreover, non-enzymatic biosensors inherently exhibit long operational life, shelf-life, or stability as they do not contain biological components that typically denature within weeks of exposure to aqueous solutions. This stability offers the possibility of a reusable glucose sensor that would not degrade with time. However, non-enzymatic biosensors typically suffer from poor selectivity, especially to electroactive species such as ascorbic acid, uric acid, and acetaminophen—chemical species found endogenously in biological fluids such as blood.

Methyl viologen (MV) may enable a path to improving sensitivity and selectivity of non-enzymatic glucose biosensors. MV has previously been used in conjunction with GOx as an electron-mediator both in solution[32] and immobilized on a sensor surface.[33] However, recent studies have shown that MV can chemically react with glucose (non-enzymatically) at a sufficiently high temperature and pH for potential use in fuel cell applications.[34] This same chemical reaction could also be used for glucose detection, such that the oxidation of reduced-MV could be correlated with the concentration of glucose, something that has never been done previously in the literature.

Herein, we have manufactured a free-standing, VACNT electrode with 16 μm diameter microchannels (~350 μm long) as a flow-through glucose sensor. A unique method of glucose detection involving a chemical reaction with MV was explored. MV was chemically reduced in the presence of glucose and was subsequently oxidized at the VACNT surface, requiring no additional surface functionalization (including no metal). Challenges with interference chemicals were mitigated by operating at a low potential of -0.2 V vs. Ag/AgCl. This MV-based VACNT sensor was compared to enzymatic VACNT electrodes functionalized by strategies typical for enzymatic glucose sensors. Unlike the MV sensor, the VACNTs of the enzymatic sensors were functionalized with Pt nano-urchins. GOx was incorporated into three different enzymatic VACNT sensors: GOx mixed into the solution, GOx covalently bound to the VACNTs, and GOx entrapped in a polymer on the CNTs. The electrochemical reaction of MV on the VACNT surface was able to produce more electrons per glucose molecule than is possible with GOx (an average of 3.4, compared to a maximum of 2). Current density was linear with flow rate for MV and GOx-in-solution sensing approaches. However, current density was not linear with flow rate when the chemical and electrochemical reactions both happened at the electrode surface, as was the case with the covalent and polymer VACNT sensors. The current density of each of the sensors was linear with glucose concentration, with the MV sensor producing the highest sensitivity and lowest limit of detection. FIA allows for a more practical application, where smaller analyte volumes can be tested by reducing the cross-sectional area of the VACNT electrode. Using MV with a small flow cell has the potential to measure glucose levels with 200 μL samples in the concentration range typical of saliva.

2. Methods

2.1. VACNT Fabrication

VACNT fabrication methods were similar to previously published protocols.[15, 35] Summarizing, 50 nm of aluminum oxide (Al_2O_3) was deposited onto a 100 mm silicon (Si) wafer by e-beam evaporation. Photolithography was used to pattern positive photoresist (AZ3330) into an array of 16 μm diameter circles that would eventually allow for the formation of defined channels. A thin (7 nm) film of iron (Fe) was thermally evaporated onto the patterned photoresist, followed by sonication in N-Methyl-2-pyrrolidone (NMP) for at least 10 minutes for lift-off patterning of Fe (see schematic in Figure 1A). The patterned wafer was diced into 17 mm squares using a diamond-coated blade.

VACNTs were grown by chemical vapor deposition (CVD) in a 1 inch diameter Lindberg/Blue M tube furnace with flowing hydrogen (H_2, 311 sccm) and ethylene (C_2H_4, 338 sccm) at 750 °C for 6 minutes. The temperature was then raised to 900 °C and the H_2 flow rate reduced to 190 sccm to infiltrate (coat) the VACNTs with amorphous carbon for 10 minutes (C_2H_4 flow rate was unchanged). This infiltration process strengthened the VACNT structure to create a mechanically sturdy, porous array of microchannels that self-released from the substrate (see geometry in Figure 1B). The resulting free-standing VACNT array (about 350 μm thick) was placed in an oxygen plasma etch for 7 minutes (5 minutes on bottom; 2 minutes on top) in a Technics Planar Etch II machine (250 W, 300 mTorr).

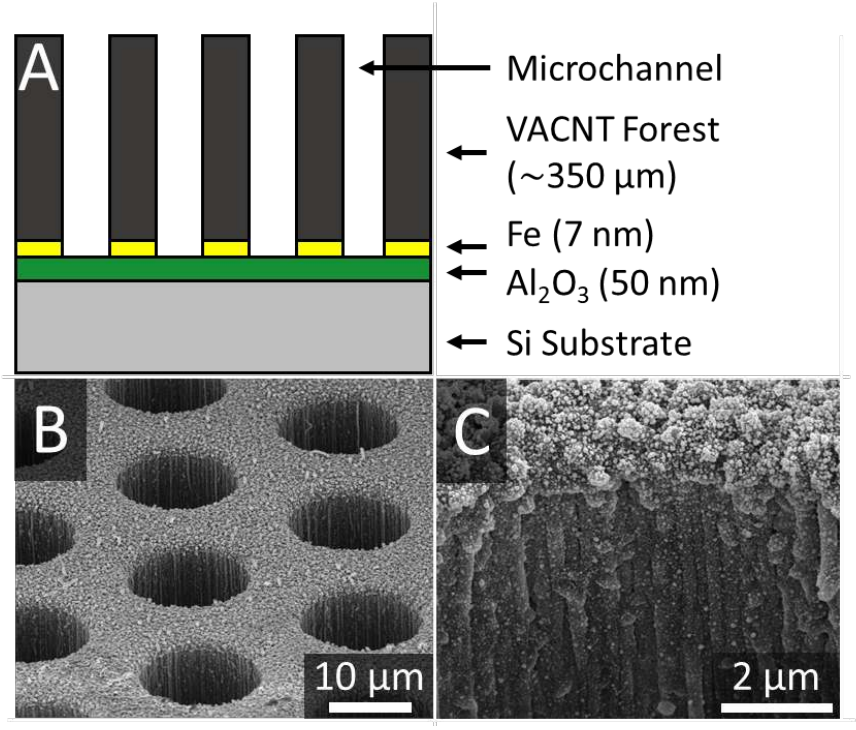

Figure 1. (A) Schematic of layers used to manufacture the VACNT sensor architecture (before self-release): Si, Al_2O_3, Fe, and VACNTs. (B) SEM image of array of VACNT microchannels with Pt. (C) SEM image near channel opening, showing Pt coverage on VACNTs.

2.2. Functionalization for Enzyme-Based Sensing

2.2.1. Platinum

The VACNTs used for enzymatic sensing were functionalized with platinum nano-urchins (PNUs) as shown in Figure 1B and C. The PNUs were deposited in a static, electroless environment by the chemical reduction of a 3 mM chloroplatinic acid hexahydrate solution (37.5% Pt, Sigma-Aldrich 206083) similar to previous protocols.[35-37] The VACNT array was held vertically in a Teflon stand for about 18 hours in a solution containing chloroplatinic acid, 18 mL of ultrapure water and 2 mL of formic acid (88% HCOOH, Macron 2592-05). After the deposition, the PNU-VACNT array was thoroughly rinsed in water and placed on a hot plate to evaporate excess liquid before measuring the Pt mass. Note that no PNUs were deposited on sensors used with MV (see Figure 2A), whereas PNUs were the only functionalization used for sensors with GOx-in-stream (see Figure 2B).

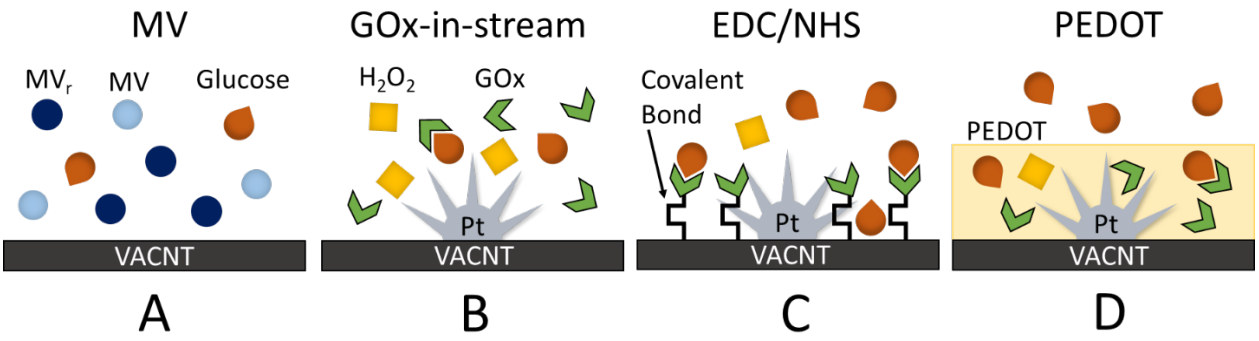

Figure 2. Various VACNT glucose sensor configurations. (A) Non-enzymatic MV sensor with no surface functionalization. (B) GOx-in-stream sensor, with Pt on the surface. (C) EDC/NHS sensor with GOx covalently bonded to the VACNTs. (D) PEDOT sensor with GOx entrapped in the polymer.

2.2.2. Covalent (EDC/NHS) Binding

Glucose oxidase from *Aspergillus niger* (GOx, type X-S, 100,000-250,000 units/g, Sigma-Aldrich G7141) was covalently bonded to the PNU-VACNT array using 1-ethyl-3-(-3-dimethylaminopropyl) carbodiimide (EDC, Sigma-Aldrich E7750) and N-hydroxysuccinimide (NHS, Sigma-Aldrich 130672) chemistry following approximately the conditions that were optimized by Wang, et al. (see Figure 2C).[38] The PNU-VACNT array was incubated in 5 mL of 50 mM EDC and 400 mM NHS in 0.1 M 2-(N-morpholino) ethanesulfonic acid (MES, pH 4.7, Thermo Scientific 28390) for 90 minutes to allow the carboxyl groups on the VACNTs to react with EDC and to form NHS esters in preparation for GOx coupling. The sample was then rinsed with ultrapure water and then placed in a 5 mL phosphate buffered saline (PBS, pH 7.4) solution with 50 mg of GOx (10 mg/mL). The EDC/NHS-PNU-VACNT array was incubated in the GOx mixture at 4 °C at least 16 hours. The GOx-EDC/NHS-PNU-VACNT (hereafter referred to as the EDC/NHS sensor) was then thoroughly rinsed and stored in PBS at 4 °C.

2.2.3. Polymer (PEDOT) Entrapment

GOx was entrapped in the polymer poly(3,4-ethylene-dioxythiophene) (PEDOT) at the PNU-VACNT surfaces following a procedure similar to that of Claussen, et al. (see Figure 2D).[7] First, 35 mg of poly(sodium 4-styrenesulfonate) (PSS, Sigma-Aldrich 243051) was stirred into 5 mL of ultra-pure water. Then, 16 µL of 3,4-ethylene-dioxythiophene (EDOT, Sigma-Aldrich 483028) was mixed into the PSS solution. Finally, 50 mg of GOx (10 mg/mL) was added to the EDOT-PSS solution. The electropolymerization of EDOT to PEDOT was performed in a flow cell (see section 2.6 below) at a flow rate of 0.1 mL/min with a multi-step current (0.5 seconds at 1 mA and

0.5 seconds at 0 A) for 500 cycles. The resulting GOx-PEDOT-PSS-PNU-VACNT (hereafter referred to as the PEDOT sensor) was thoroughly rinsed and stored in PBS at 4 °C.

2.3. Amperometric Measurements and Environments

All experiments were performed in a flow-through electrochemical cell (see section 2.4) with a saturated (KCl) Ag/AgCl reference electrode, a Pt wire counter electrode, and a VACNT microchannel array as the working electrode. A CH Instruments (CHI) 660E Potentiostat/Galvanostat was employed for all electrochemical testing. Before experiments were performed, a potential (see below for values) was applied to the VACNT electrode until a steady current density was obtained.

2.3.1. Glucose Oxidase

Glucose (Dextrose, Sigma-Aldrich D9434) oxidation with GOx took place under a constant potential of 0.55 V relative to Ag/AgCl in phosphate buffered saline (1X PBS, pH 7.4, Fisher Scientific) at room temperature and typical air exposure. The two-part reaction converted glucose into hydrogen peroxide (H_2O_2) as shown in Eq. 1 and then the H_2O_2 was oxidized at the PNU-VACNT surface to produce two electrons as shown by Eq. 2 (equilibrium potential of 0.204 V vs. Ag/AgCl at pH 7.4).[39]

$$\text{D-glucose} + O_2 + H_2O \rightarrow \text{D-gluconic acid} + H_2O_2 \qquad \text{Eq. 1}$$

$$H_2O_2 \rightarrow O_2 + 2H^+ + 2e^- \qquad \text{Eq. 2}$$

2.3.2. Methyl Viologen

For the non-enzymatic detection of glucose, methyl viologen dichloride hydrate (MV, 98%, Fisher Scientific) was used to chemically react with glucose to produce reduced-MV (MV_r). For this reaction to occur at relevant rates, it was required to increase both temperature and pH,[34] with optimal conditions at 55 °C (at a 60 °C set point) and pH 13 (using 0.1 M NaOH). In a basic electrolyte, glucose experiences an enolization process where glucose molecules are converted into endiolate anions, as shown in Eq. 3 (where D-glucose* represents the endiolate species).[40-41] The endiolate species react with MV (the oxidized form of the catalyst) where MV reduces to MV_r (Eq. 4). Under this oxidation reaction, the endiolate species then convert into various products that depends on the oxidation extent of the glucose.

$$\text{D-glucose} + OH^- \rightarrow \text{D-glucose}^* \quad \text{Eq. 3}$$

$$\text{D-glucose}^* + MV \rightarrow MV_r + \text{products} \quad \text{Eq. 4}$$

The produced MV_r is a free species in the electrolyte which is subsequently oxidized directly on the VACNT surface at a potential of -0.2 V vs. Ag/AgCl without the presence of platinum or any other functionalization on the VACNT structure following Eq. 5 (standard potential of -0.644 V vs. Ag/AgCl, converted from SCE[42]).

$$MV_r \rightarrow MV + e^- \quad \text{Eq. 5}$$

Note that MV in Eq. 5 represents oxidized-MV, returning to its original state before being reduced by glucose.

MV experiments were performed in an anaerobic glovebox to prevent oxidation of MV_r, which oxidizes readily in atmospheric conditions with oxygen. Glucose-NaOH solution in 15 mL test tubes (varying concentrations, including a control without glucose) was held in a water bath for about 10 minutes, after which MV was added (1 mM MV) and allowed to react for 20 minutes before introducing the solution into the flow-through set up.

2.4. Flow Cell Configurations

The larger electrochemical flow cell is shown in Figure 3A, where the VACNT sensor was held between two, size-12 O-rings (3/8" ID) in a clamped Teflon flow cell. Forced mechanical contact between the VACNT electrode and a Nichrome wire allowed for a simple connection mechanism. The flow cell was oriented vertically, with the reference electrode upstream and the counter electrode downstream of the VACNT, each held in place by bored out rubber stoppers. A 60 mL syringe pulled solution through the cell from a reservoir using a Harvard Apparatus PHD Ultra syringe pump to control the flow rate. New pre-mixed concentrations of glucose solution were added to the open reservoir as the previous solution emptied from the reservoir. At high glucose concentrations (>500 μM), the syringe pump was operated in infuse mode instead of withdraw mode to allow bubbles formed at the electrode to escape (only relevant with GOx sensors as no bubbles formed from MV).

Figure 3B shows an application of the VACNT sensor at a much smaller scale, where glucose can be injected into the stream (FIA) instead of being pre-mixed in the solution. A much smaller

cross-section of VACNT electrode was positioned between two pieces of 1/16" ID (1/8" OD) PVC tubing and held together by 1/8" ID (3/16" OD) tubing. A T-connector was used to allow the reference electrode access to the solution, which was also held in place by 1/8" ID tubing. The solution was pushed (infused) through at a rate of 0.2 mL/min. A 200 µL sample of glucose was manually injected upstream into the tubing over approximately 4 seconds (~3 mL/min).

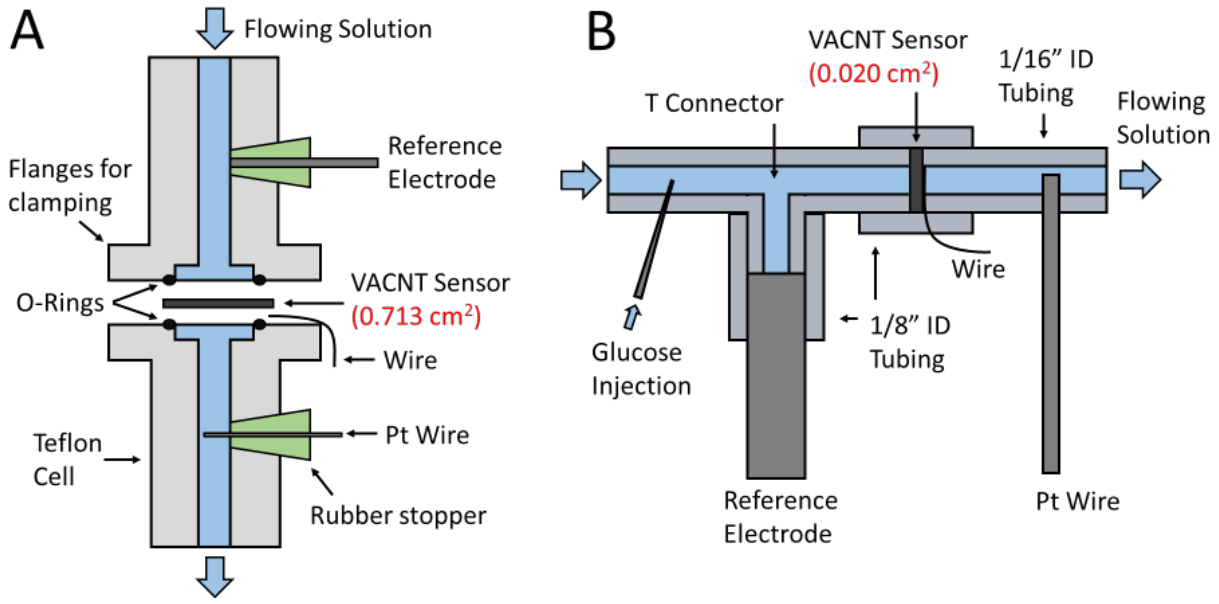

Figure 3. Schematic of (A) large and (B) small flow-through cells, where the chemical solution is forced through the VACNT microchannels. The small flow cell enables FIA of 200 µL of glucose.

3. Results and Discussion

3.1. Characterization

VACNT heights (electrode thicknesses) were measured to be 351 ± 27 µm. With a nominal channel diameter of 16 µm, the channel length to diameter ratio was about 22. The nominal void ratio of each electrode was 0.41. VACNTs coated with amorphous carbon have been shown to have a high number of surface defects that are favorable for increasing charge transfer, as previously shown by Raman spectroscopy.[43]

For the enzymatic sensors, the mass of the deposited Pt was measured to be 4.46 ± 0.70 mg (14.7 ± 2.3 % of sensor by weight). More detailed characterization of Pt deposited in a similar manner can be found by others, including analysis by TEM[35] and XRD.[44]

3.2. MV Wait Time

For the chemical reaction of glucose with MV, a maximum pH of 12 is recommended by Watt because MV becomes unstable at high pH.[34] However, it was found that at relatively low MV concentrations (1 mM), MV could be used in a pH 13 solution (0.1 M NaOH) because the rate of MV decomposition was negligible compared to the glucose-MV reaction. Thus, a pH 13 solution was chosen to provide faster reaction rates of glucose and reduce the waiting time. To determine the optimal waiting time for the reaction, the current was measured in the large flow cell in 10 min intervals (data not shown). A maximum current was obtained at 30 minutes, with 82% of the maximum at 10 minutes and 97% of the maximum at 20 minutes. Longer times (40 and 50 minutes) resulted in a slight decrease in the measured current. Thus, a 20-minute wait time was chosen for all subsequent experiments.

3.3. Flow Rate

Flow rate greatly influences the sensitivity of flow sensors and can provide linearly varying current with flow rate.[15] Figure 4 shows the measured current density for 100 μM glucose at different volumetric flow rates (0.5 to 8 mL/min; average velocities: 0.283 to 4.53 mm/s) for each of the glucose sensors (MV, GOx-in-stream, EDC/NHS, and PEDOT; see Figure 2) in the large flow cell. A concentration of 100 μM glucose was chosen to mimic a typical glucose concentration found in saliva and is representative of an accessible bodily fluid with a lower concentration. The current was normalized by the frontal surface area, as defined by the O-rings (0.713 cm^2).

Figure 4A shows that the current density was largest and most linear with flow rate when the glucose reaction occurred upstream of the VACNT electrode, as was the case with both GOx and MV in solution. The green dashed line represents the current density that would be obtained for 100 μM glucose (at the given flow rate) if each glucose molecule produced two electrons. This becomes the theoretical maximum for GOx reactions if each glucose molecule was converted into H_2O_2 and then each H_2O_2 molecule reacted at the surface (see Eqs. 1 and 2). However, when the GOx was in the stream, a reaction efficiency of glucose to H_2O_2 was observed, as the current

density was only about 64% the theoretical values. On the other hand, the MV reaction produced a significantly higher current density, at approximately 2.65 times the current density produced with GOx in stream, resulting in an average of 3.4 electrons per glucose molecule. This is possible because it is not H_2O_2, but MV_r, that is oxidized at the electrode surface (see Eq. 5). Tests were repeated for three separate VACNT sensors with an average standard deviation relative to the mean of 11.9%. It should be noted that the lowest flow rate gave a much higher relative standard deviation of 31.5% and was likely due to experimental error.

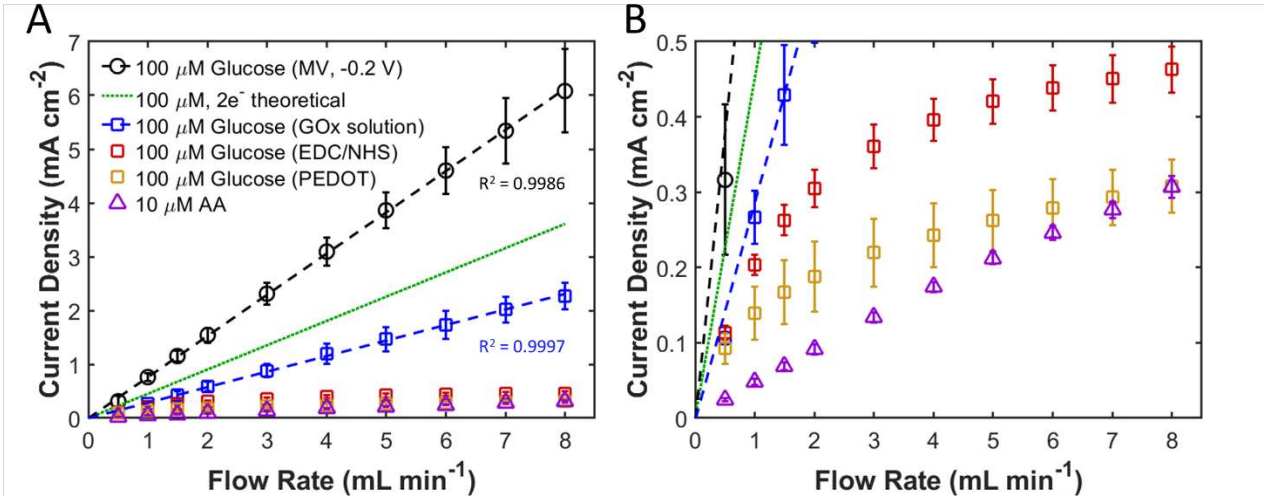

Figure 4. (A) Comparison of current density from 100 µM glucose for different VACNT electrodes at various flow rates (0.5 – 8 mL/min). The current density from MV and GOx-in-stream sensors were both linear with flow rate, with the MV sensor collecting more than 2 electrons per glucose molecule. The MV sensor operated at -0.2 V vs. Ag/AgCl in 0.1 M NaOH, while the remainder of the sensors were tested at 0.55 V vs. Ag/AgCl in pH 7.4 PBS. The current density from ascorbic acid (AA) at 0.55 V vs. Ag/AgCl is also shown. (B) Close up of low current density measurements, showing that the EDC/NHS and PEDOT sensors were nonlinear with flow rate. Note that error bars represent standard deviation from three repeat measurements.

When the chemical reaction was moved to the electrode by functionalizing the VACNTs with GOx, a nonlinear trend with flow rate was observed (see Figure 4B). At the lowest flow rate tested (0.5 mL/min), the current density of each of the GOx sensors was very similar, but the current densities of the functionalized sensors begin to asymptote as flow rate increases. This suggests that the time component to the two-part reaction of glucose with GOx and H_2O_2 with the PNU-VACNT surface becomes significant at high flow rates. For example, at 0.5 mL/min there would be on average 1.24 seconds to complete the chemical and electrochemical reactions within the VACNT

array, but only 0.08 seconds at 8 mL/min. When the chemical reaction takes place before reaching the electrode, only the electrochemical portion needs to take place during this time. Although both the EDC/NHS and PEDOT sensors follow the same trend, it can also be seen in Figure 4B that the EDC/NHS sensor exhibited higher current densities at higher flow rates (about 1.5 times larger at 8 mL/min). The lower current from the PEDOT sensor could be caused from less coverage of GOx as a result of the polymer functionalization, or because the polymer layer acts as a diffusion barrier between the VACNT surface and the solution. It is also possible that variations in PEDOT coverage and VACNT channel length caused the PEDOT sensor to have the largest average standard deviation relative to the mean at 18.8%.

Flow rates for subsequent concentration tests were chosen to yield large current densities while still maintaining reasonable solution volumes. For GOx functionalized on the VACNTs, it is most efficient to be below 3 mL/min at a concentration of 100 μM because current doesn't increase significantly with flow above this point. A flow rate of 1 mL/min was chosen because the EDC/NHS current density was still close to the GOX-in-stream current density at this point and for reasons discussed in the following section on selectivity (see section 3.4). For the in-solution sensors, the selection of flow rate is somewhat arbitrary as sensitivity will continue to increase with increasing flow rate. To maintain reasonable solution volumes, a flow rate of 6 mL/min was chosen.

3.4. Selectivity

3.4.1. Enzyme Sensors

Selectivity of glucose against interfering species is important for the accurate measurement of glucose concentrations. Also shown in Figure 4 is current density with flow rate for 10 μM of ascorbic acid (AA, Fisher Scientific) at a potential of 0.55 V vs. Ag/AgCl (same as GOx tests), as tested with each of the GOx sensors (Pt only, EDC/NHS, and PEDOT). The current density from this interfering species was rather large because AA oxidizes readily at this potential.[45] This was especially significant for the low current densities of EDC/NHS and PEDOT sensors at high flow rates, which is the main reason to operate the functionalized sensors at a low flow rate (1 mL/min). GOx-in-stream had the least impact, with the 10 μM AA giving a current density about 15% of the 100 μM glucose current density (minimal dependence on flow rate). At lower potentials, it is possible to minimize the effects of interfering species and measure the change in the O_2 reduction

current.[45] However, at low potentials the PNU-VACNTs produced a very large negative current from the reduction of oxygen, making it unreasonable to operate at low potentials in the presence of oxygen (oxygen is required for the GOx reaction).

It has previously been shown that a polymer layer such as PEDOT can help reduce the impact from interfering species[7]. However, the current density was nearly identical with and without the PEDOT layer on the PNU-VACNT electrodes, as the small standard deviation in Figure 4B includes both PEDOT and non-PEDOT samples. It is possible that the large surface area and high-aspect-ratio VACNT channels were not completely coated with the polymer and the resulting electrode was thus able to oxidize the interfering species at the same rate as the sensors with PEDOT.

3.4.2. MV Sensor

With MV there was more flexibility in the operating potential of the sensor because tests were performed in an oxygen-free environment (avoiding the current from oxygen reduction while preventing the oxidation of MV_r) and because the standard equilibrium potential of MV is very low (-0.644 vs. Ag/AgCl, converted from SCE[42]). It was observed that a significant current was produced by interfering species on the VACNT electrode at potentials above about -0.2 V vs. Ag/AgCl, below which the current from the interfering species was significantly lower (data not shown). Thus, a potential of -0.2 V vs. Ag/AgCl was chosen for all experiments with MV.

Figure 5 shows the impact of interfering species on the current density of 100 μM glucose with 1 mM MV. The initial baseline is from heated 0.1 M NaOH and 1 mM MV flowing at 6 mL/min, followed by the upstream addition of heated NaOH with 100 μM glucose and 1 mM MV at ~100 s. As this upstream solution was depleted, a comparable mixture was added to the upstream reservoir at ~210 s, now with several interfering chemicals present (NaOH heated with 100 μM glucose, 10 μM AA, 10 μM uric acid (UA, Sigma-Aldrich U2625), 10 μM acetaminophen (AP, Sigma-Aldrich A5000) and 1 mM MV). In this manner, the ability to detect glucose in the presence of the interfering chemicals was demonstrated. There was an observed increase in current density of about 6% from the three interfering species combined, likely caused by a slight reaction with MV. It should be noted that a small oscillation in the measured current was observed after the addition of glucose, as can be seen in Figure 5. The oscillations corresponded to the stepping of the syringe pump, a phenomenon previously observed in the signal for H_2O_2 detection.[15]

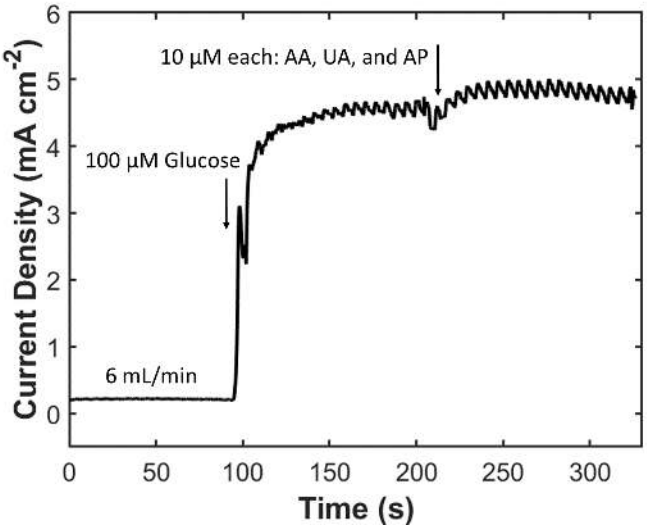

Figure 5. Current density with time for 100 µM glucose and 1 mM MV in 0.1 M NaOH flowing at 6 mL/min and potential of -0.2 V vs. Ag/AgCl, followed by an upstream addition of 10 µM of each of the following common interfering species: ascorbic acid (AA), uric acid (UA) and acetaminophen (AP). A 6% increase in current was observed by the addition of interfering species with the glucose.

3.5. Sensitivity, Limit of Detection, and Linear Sensing Range

The current density with time at lower concentrations of glucose (2.5 to 10 µM) with MV is shown in Figure 6. The baseline is heated NaOH and 1 mM MV flowing at 6 mL/min, followed by the upstream additions of heated NaOH with glucose and 1 mM MV. At these low concentrations, there is still a distinct increase in current with the addition of glucose and a linear relationship between current density and glucose concentration is apparent.

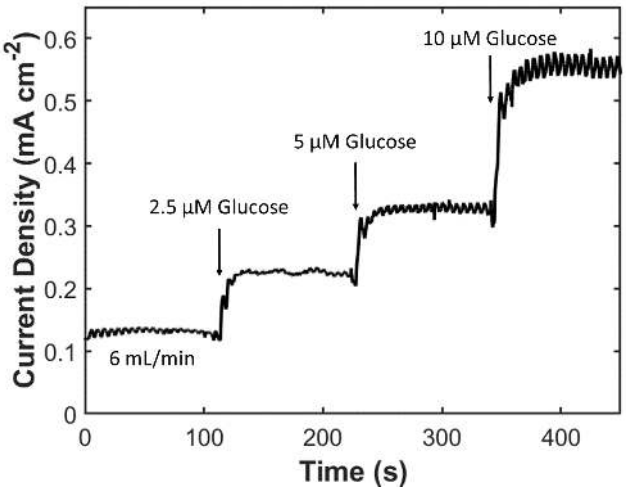

Figure 6. Current density with time for low glucose concentrations (2.5, 5, 10 µM) with 1 mM MV in 0.1 M NaOH at a flow rate of 6 ml/min and potential of -0.2 V vs. Ag/AgCl.

Figure 7 shows the current density at various glucose concentrations for MV, GOx-in-solution, and EDC/NHS sensors. The PEDOT sensor was not included in the concentration experiments because it showed no advantage over the EDC/NHS sensor from the flow rate experiments in section 3.3. In Figure 7A the full linear range of the EDC/NHS sensor is shown to be much larger than the other two sensors, up to about 6 mM glucose. The MV and GOx-in-solution sensors both reach their linear limit at about 200 µM glucose. It is likely that the EDC/NHS electrode had a much larger linear range because it was operating at a much lower flow rate. Thus, it seems that the flow rate of the sensor could potentially be modified to target different concentration ranges with a linear response.

Figure 7B shows the linear range for the MV and GOx-in-solution sensors. It can be seen that each sensor is linear below 200 µM glucose, with MV having the largest slope and thus the highest sensitivity at 45.93 mA mM^{-1} cm^{-2} (based on the projected frontal area of 0.713 cm^2). The limit of detection (LOD) of each sensor was calculated from the sensitivity (based on three times the standard deviation of the baseline), with the observed lowest linear sensing region being slightly higher than the LOD. The MV sensor had the lowest LOD at 100 nM glucose and was linear down to a concentration of 250 nM.

Table **1** summarizes the measured performance of each VACNT sensor, including the sensitivity, LOD, and linear range. The low limits of detection and high sensitivities for the VACNT sensors shown in

Table **1** are comparable with the best glucose sensors in the literature, with glucose sensors typically ranging from 5 to 100,000 nM glucose LOD and sensitivities of 0.001 to 12 mA mM^{-1} cm^{-2}.[9, 14, 28, 46] The large sensitivity of the VACNT sensors comes from high current per geometric cross-sectional area and does not include the surface area associated with microchannel length. It is interesting to note that although the sensitivity of the EDC/NHS sensor was much lower, the background noise was nearly proportionally smaller, such that the calculated limit of detection was still very similar to that of the other sensors. With GOx in solution, the background noise was significantly higher than that for PBS alone. Although the EDC/NHS sensor operated at a slower flow rate of 1 mL/min, it would have only marginally increased sensitivity if operated at 6 mL/min, as noted in section 3.3.

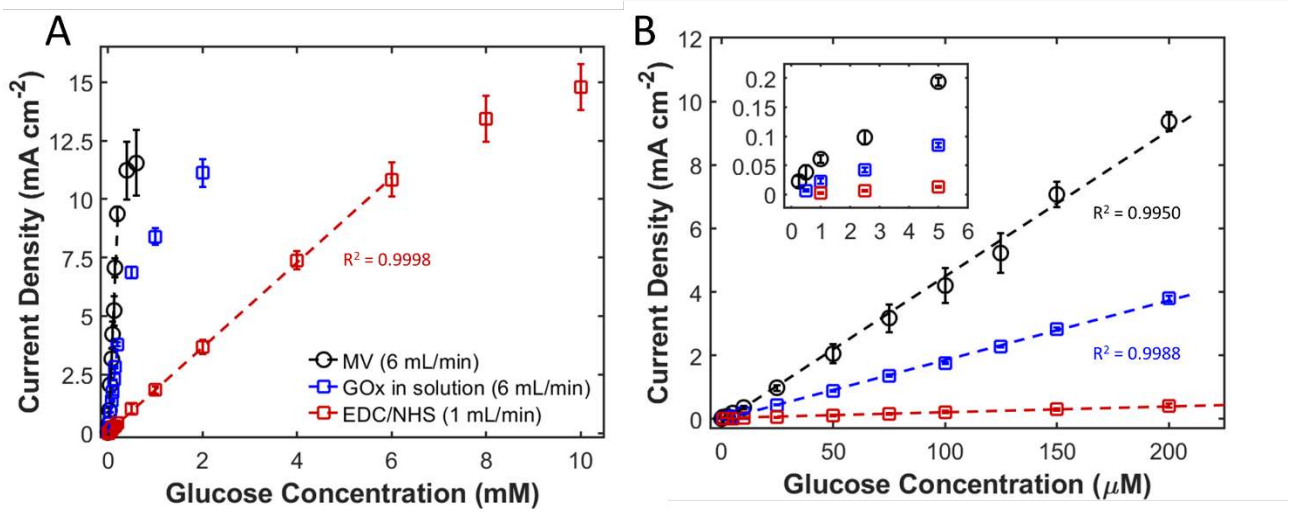

Figure 7. Measured current density at different glucose concentrations flowing at 1 mL/min for EDC/NHS sensors and 6 mL/min for MV and GOx-in-solution. The MV sensor operated at -0.2 V in 0.1 M NaOH, while GOx-in-solution and EDC/NHS sensors were tested at 0.55 V in pH 7.4 PBS. (A) Full linear range of EDC/NHS sensor is shown to be much larger than the linear range of GOx-in-solution and MV. (B) Current density for lower glucose concentrations, where all of the sensors are linear and MV has the highest current density for any given concentration. Inset: Linear sensing range as low as 0.25 μM. Note that error bars represent standard deviation from three repeat measurements.

Table 1: Summary of various VACNT sensor conditions and measured results in this work.

Sensor	Potential* (V (Ag/AgCl))	Flow Rate† (mL/min)	Sensitivity‡ (mA mM^{-1} cm^{-2})	LOD (nM)	Linear Range (μM)
MV	-0.2	6	45.93	100	0.25 to 200
GOx-in-solution	0.55	6	18.77	194	0.5 to 200
EDC/NHS	0.55	1	1.815	311	1 to 6,000
Small MV	-0.2	0.2	5.002	360	<50 to >150§

*Chosen to produce high glucose signal while reducing signal from interfering species (see section 3.4)

[†]Selected based on linearity and solution volume limitations as noted in section 3.3
[‡]Based on projected frontal area of 0.713 cm^2 (or 0.020 cm^2 for small MV sensor)
[§]Linearity beyond this range was not explored

3.6. Small Volume MV Sensor

A smaller flow cell (see Figure 3B) was used to demonstrate glucose detection with much smaller volumes (200 µL) via flow injection analysis (FIA). The cross-sectional area was reduced by 36 times, giving an area of only 0.020 cm^2 (compared to 0.713 cm^2). A flow rate of 0.2 mL/min was chosen, giving an average velocity of 4.08 mm/s. This velocity through the smaller sensor was comparable to that for the larger flow cell (equivalent to a large cell flow rate of 7.2 mL/min). However, during glucose injection the velocity increased as the 200 µL sample was injected over about 4 seconds (about 3 mL/min). The overall flow rate through the small sensor would then be ~3.2 mL/min, suggesting that the solution concentration would be approximately 95% of the injected glucose concentration.

Figure 8A shows the current density with time during the injection of different glucose concentrations (0, 50, 100, 150 µM) and 1 mM MV. The conditions were the same used with MV in the large flow cell: a 20-minute wait time in pH 13 (0.1 M) NaOH, with the VACNT electrode at a potential of -0.2 V. Two injections are shown for each concentration, with a close up of a single injection shown in the figure inset. There was a high current density measured during the glucose injection period (about 4 seconds). After the injection, there was a steady region with a high glucose concentration at the original flow rate (0.2 mL/min) before the current density reduced to the baseline current.

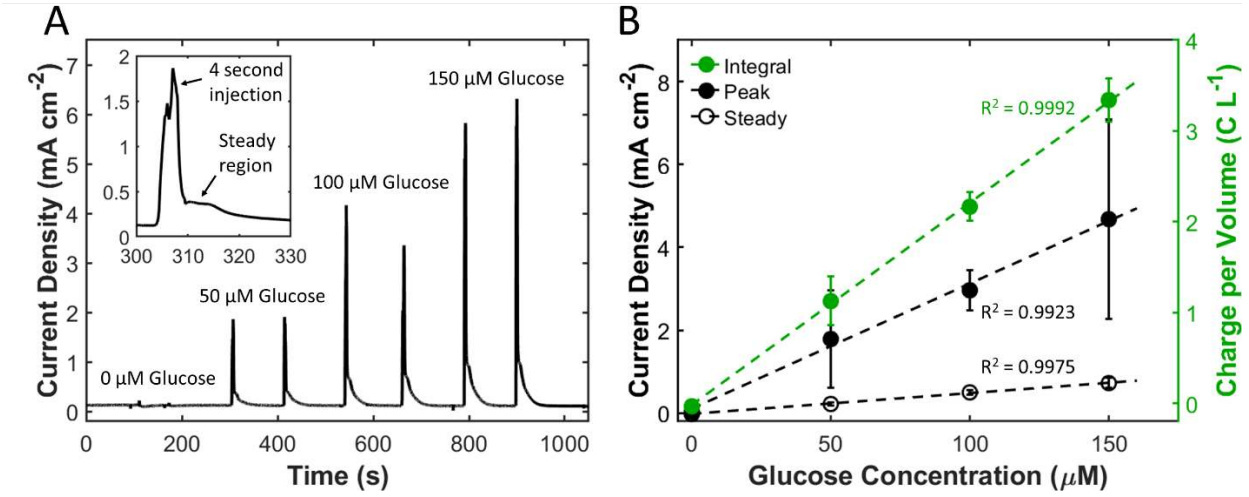

Figure 8. Small volume flow cell with 200 µL injections of glucose (0, 50, 100, 150 µM) and 1 mM MV flowing at 0.2 mL/min and operating at -0.2 V in 0.1 M NaOH. (A) Current density from two injections of each concentration as a function of time. Inset: Zoomed view of 50 µM injection, showing the peak caused by injection and a steady region before reducing to baseline current. (B) Methods used to detect glucose concentration including integration of current from injected glucose (normalized by injection volume), peak current density during injection, and steady current density just after injection. Each method is linear with concentration with the peak current density measurements exhibiting the largest standard deviation. Note that error bars represent standard deviation from the average of two tests for three repeat devices.

With this FIA, there are three different values that can be used to correlate to glucose concentration: (1) integration of the current to obtain total charge (normalized by the injection volume), (2) measured peak current density during injection, and (3) measured steady current density after the injection. Figure 8B shows that each of these measurement techniques was linear with glucose concentration. However, a larger standard deviation of peak current density was observed (44.6% average standard deviation relative to the mean), compared to the steady region current density (15.5%). The large standard deviation of the peak current density was likely due to manual control of the injection rate, where the rate of injection greatly influenced the peak current densities.

Although the current-integration method is a valid calculation method, by using the current density measured in the steady region it was possible to determine a sensitivity and limit of detection that could be compared with the large flow cell. The sensitivity from the curve fit slope was determined to be 5.002 mA cm^{-2} mM^{-1}, which is about 9 times smaller than the sensitivity of the large flow cell. Although a larger sensitivity could be obtained using the peak current density, the measured signal was much more variable than the steady current density, as noted by the large error bars in Figure 8B.

With a smaller sensor also came much smaller background noise, which resulted in a calculated limit of detection (LOD) of 360 nM glucose. Thus, although the sensitivity was less than the large MV sensor, the smaller background noise helped give a comparable LOD. The full linear range was not investigated for the smaller sensor, but experiments demonstrate that the measurement was linear with concentration up to at least 150 μM glucose. Within this concentration range and with as little as 200 μL (or potentially less) the MV sensor has the potential to measure the glucose levels found in saliva.[22]

Table **1** reports the measured performance of the small sensor as compared to the other sensors in this work.

3.7. Advantages and Disadvantages of MV for Glucose Sensing

MV has been shown to be a promising agent for enhancing glucose detection. Because the chemical reaction does not involve a pathway with H_2O_2, it is possible to detect more than 2 electrons per glucose molecule. This led to a very high sensitivity with a low limit of detection for both the large bulk experiments and for the small volume FIA experiments. Also, no additional functionalization of the sensor was necessary, as the electrode consisted of only carbon (VACNTs with added carbon from the infiltration process). This means that no metal was needed and also no enzyme was necessary, avoiding typical problems of enzymatic sensors, such as signal decay in time. The low working potential also allowed for minimizing the effect of interfering species.

The advantages of using MV come at a potential cost, as the MV sensor exhibits a few key restrictions when compared to GOx-based sensors. The temperature of the solution was elevated to 55 °C in order to facilitate the reaction of MV with glucose and was allowed to proceed for 20 minutes in an oxygen-free environment before measuring the current. The solution was also at pH 13, likely requiring an increase in solution pH, similar to many other non-enzymatic sensors. While these conditions may be challenging to implement and are limited to in vitro applications, the idea of utilizing an amplification chemical to react with glucose is an intriguing prospect.

4. Conclusions

This work has shown the effectiveness of using MV as the reacting agent for glucose detection. When combined with the VACNT electrode, the measured current density from the non-enzymatic MV reaction was very high (with a sensitivity of 45.93 mA mM^{-1} cm^{-2} and a limit of

detection of 100 nM). These high current densities were linear with both flow rate and glucose concentration in the 0.25–200 μM range and the effect from common interfering species was minimal at the low working voltage of -0.2 V vs. Ag/AgCl. Future work will involve investigating the interference from carbohydrates other than glucose. MV-based glucose sensing is potentially limited in self-glucose monitoring applications due to the chemical reaction of glucose with MV at an elevated temperature in an oxygen-free environment for several minutes before passing though the sensing electrode.

With surface-based, enzymatic GOx reactions, the measured current density leveled off at lower flow rates than for sensors that allowed the chemical reaction to take place in solution. For convective-enhanced sensor technologies, the additional requirement of having all of the chemical reactions taking place at the sensor surface introduces an additional limitation in utilizing flow rate to increase sensor sensitivity. Further, measured current densities with MV were higher than theoretically possible with enzymatic GOx reactions, with a release of 3.4 electrons per glucose molecule on average. The additional electrons made available with MV in this flowing configuration may also be useful in increasing power output of glucose-based biofuel cells.

The MV sensor was scaled down in size to enable the detection of glucose in small volumes of only 200 μL. The small sensor had a high enough sensitivity to potentially measure glucose levels found in saliva, with testing in real saliva samples as an area for future investigation. The small VACNT configuration could also be applied to enzymatic sensors, with potential future work including the exploration of injection-based, small volume sensing with VACNT electrodes to enhance enzymatic sensing.

Acknowledgements

The authors gratefully acknowledge support from the Department of Mechanical Engineering and College of Engineering and Technology at Brigham Young University.

References

(1) Sattayasamitsathit, S.; Gu, Y.; Kaufmann, K.; Jia, W.; Xiao, X.; Rodriguez, M.; Minteer, S.; Cha, J.; Burckel, D. B.; Wang, C.; Polsky, R.; Wang, J. Highly Ordered Multilayered 3D Graphene Decorated with Metal Nanoparticles. *Journal of Materials Chemistry A* **2013,** *1* (5), 1639-1645, DOI: 10.1039/C2TA00954D.

(2) Bandodkar, A. J.; Jeerapan, I.; You, J.-M.; Nuñez-Flores, R.; Wang, J. Highly Stretchable Fully-Printed CNT-Based Electrochemical Sensors and Biofuel Cells: Combining Intrinsic

and Design-Induced Stretchability. *Nano Letters* **2016,** *16* (1), 721-727, DOI: 10.1021/acs.nanolett.5b04549.
(3) Gupta, S.; Murthy, C. N.; Prabha, C. R. Recent Advances in Carbon Nanotube Based Electrochemical Biosensors. *International Journal of Biological Macromolecules* **2018,** *108*, 687-703, DOI: 10.1016/j.ijbiomac.2017.12.038.
(4) Claussen, J. C.; Franklin, A. D.; Haque, A. U.; Marshall Porterfield, D.; Fisher, T. S. Electrochemical Biosensor of Nanocube-Augmented Carbon Nanotube Networks. *ACS Nano* **2009,** *3* (1), 37-44, DOI: 10.1021/nn800682m.
(5) Ashkan, K.; Nataliia, G.; Maria, G.; Evgeny, K. Graphene-Functionalized 3D-Carbon Fiber Electrodes – Preparation and Electrochemical Characterization. *Electroanalysis* **2016,** *28* (9), 1943-1946, DOI: 10.1002/elan.201600110.
(6) Lawal, A. T. Progress in Utilisation of Graphene for Electrochemical Biosensors. *Biosensors and Bioelectronics* **2018,** *106*, 149-178, DOI: 10.1016/j.bios.2018.01.030.
(7) Claussen, J. C.; Kumar, A.; Jaroch, D. B.; Khawaja, M. H.; Hibbard, A. B.; Porterfield, D. M.; Fisher, T. S. Nanostructuring Platinum Nanoparticles on Multilayered Graphene Petal Nanosheets for Electrochemical Biosensing. *Advanced Functional Materials* **2012,** *22* (16), 3399-3405, DOI: 10.1002/adfm.201200551.
(8) Bollella, P.; Fusco, G.; Tortolini, C.; Sanzò, G.; Favero, G.; Gorton, L.; Antiochia, R. Beyond Graphene: Electrochemical Sensors and Biosensors for Biomarkers Detection. *Biosensors and Bioelectronics* **2017,** *89*, 152-166, DOI: 10.1016/j.bios.2016.03.068.
(9) Dhara, K.; Mahapatra, D. R. Electrochemical Nonenzymatic Sensing of Glucose Using Advanced Nanomaterials. *Microchimica Acta* **2018,** *185* (1), 49, DOI: 10.1007/s00604-017-2609-1.
(10) Tsentalovich, D. E.; Headrick, R. J.; Mirri, F.; Hao, J.; Behabtu, N.; Young, C. C.; Pasquali, M. Influence of Carbon Nanotube Characteristics on Macroscopic Fiber Properties. *ACS Applied Materials & Interfaces* **2017,** *9* (41), 36189-36198, DOI: 10.1021/acsami.7b10968.
(11) Kumar, S.; Rani, R.; Dilbaghi, N.; Tankeshwar, K.; Kim, K.-H. Carbon Nanotubes: A Novel Material for Multifaceted Applications in Human Healthcare. *Chemical Society Reviews* **2017,** *46* (1), 158-196, DOI: 10.1039/C6CS00517A.
(12) Ahmad, R.; Ahn, M.-S.; Hahn, Y.-B. A Highly Sensitive Nonenzymatic Sensor Based on Fe2O3 Nanoparticle Coated ZnO Nanorods for Electrochemical Detection of Nitrite. *Advanced Materials Interfaces* **2017,** *4* (22), 1700691, DOI: doi:10.1002/admi.201700691.
(13) Ahmad, R.; Tripathy, N.; Ahn, M.-S.; Hahn, Y.-B. Solution Process Synthesis of High Aspect Ratio ZnO Nanorods on Electrode Surface for Sensitive Electrochemical Detection of Uric Acid. *Scientific Reports* **2017,** *7*, 46475, DOI: 10.1038/srep46475.
(14) Zaidi, S. A.; Shin, J. H. Recent Developments in Nanostructure Based Electrochemical Glucose Sensors. *Talanta* **2016,** *149*, 30-42, DOI: 10.1016/j.talanta.2015.11.033.
(15) Brownlee, B. J.; Marr, K. M.; Claussen, J. C.; Iverson, B. D. Improving Sensitivity of Electrochemical Sensors with Convective Transport in Free-standing, Carbon Nanotube Structures. *Sensors and Actuators B: Chemical* **2017,** *246*, 20-28, DOI: 10.1016/j.snb.2017.02.037.
(16) Amatatongchai, M.; Sroysee, W.; Chairam, S.; Nacapricha, D. Amperometric Flow Injection Analysis of Glucose Using Immobilized Glucose Oxidase on Nano-Composite Carbon Nanotubes-Platinum Nanoparticles Carbon Paste Electrode. *Talanta* **2017,** *166*, 420-427, DOI: 10.1016/j.talanta.2015.11.072.

(17) Dashty, M. A Quick Look at Biochemistry: Carbohydrate Metabolism. *Clinical Biochemistry* **2013,** *46* (15), 1339-1352, DOI: 10.1016/j.clinbiochem.2013.04.027.
(18) *IDF Diabetes Atlas, 8th edn.*, International Diabetes Federation: Brussels, Belgium, 2017.
(19) Domingueti, C. P.; Dusse, L. M. S. A.; Carvalho, M. d. G.; de Sousa, L. P.; Gomes, K. B.; Fernandes, A. P. Diabetes Mellitus: The Linkage Between Oxidative Stress, Inflammation, Hypercoagulability and Vascular Complications. *Journal of Diabetes and Its Complications* **2016,** *30* (4), 738-745, DOI: 10.1016/j.jdiacomp.2015.12.018.
(20) Klonoff, D. C.; Ahn, D.; Drincic, A. Continuous Glucose Monitoring: A Review of the Technology and Clinical Use. *Diabetes Research and Clinical Practice* **2017,** *133*, 178-192, DOI: 10.1016/j.diabres.2017.08.005.
(21) Viswanath, B.; Choi, C. S.; Lee, K.; Kim, S. Recent Trends in the Development of Diagnostic Tools for Diabetes Mellitus Using Patient Saliva. *TrAC Trends in Analytical Chemistry* **2017,** *89*, 60-67, DOI: 10.1016/j.trac.2017.01.011.
(22) Gupta, S.; Sandhu, S. V.; Bansal, H.; Sharma, D. Comparison of Salivary and Serum Glucose Levels in Diabetic Patients. *Journal of Diabetes Science and Technology* **2015,** *9* (1), 91-96, DOI: 10.1177/1932296814552673.
(23) Zhao, C.-e.; Gai, P.; Song, R.; Chen, Y.; Zhang, J.; Zhu, J.-J. Nanostructured Material-Based Biofuel Cells: Recent Advances and Future Prospects. *Chemical Society Reviews* **2017,** *46* (5), 1545-1564, DOI: 10.1039/C6CS00044D.
(24) Gamella, M.; Koushanpour, A.; Katz, E. Biofuel Cells – Activation of Micro- and Macro-Electronic Devices. *Bioelectrochemistry* **2018,** *119*, 33-42, DOI: 10.1016/j.bioelechem.2017.09.002.
(25) Cosnier, S.; J. Gross, A.; Le Goff, A.; Holzinger, M. Recent Advances on Enzymatic Glucose/Oxygen and Hydrogen/Oxygen Biofuel Cells: Achievements and Limitations. *Journal of Power Sources* **2016,** *325*, 252-263, DOI: 10.1016/j.jpowsour.2016.05.133.
(26) Abreu, C.; Nedellec, Y.; Gross, A. J.; Ondel, O.; Buret, F.; Goff, A. L.; Holzinger, M.; Cosnier, S. Assembly and Stacking of Flow-through Enzymatic Bioelectrodes for High Power Glucose Fuel Cells. *ACS Applied Materials & Interfaces* **2017,** *9* (28), 23836-23842, DOI: 10.1021/acsami.7b06717.
(27) Sassolas, A.; Blum, L. J.; Leca-Bouvier, B. D. Immobilization Strategies to Develop Enzymatic Biosensors. *Biotechnology Advances* **2012,** *30* (3), 489-511, DOI: 10.1016/j.biotechadv.2011.09.003.
(28) Mross, S.; Pierrat, S.; Zimmermann, T.; Kraft, M. Microfluidic Enzymatic Biosensing Systems: A Review. *Biosensors and Bioelectronics* **2015,** *70*, 376-391, DOI: 10.1016/j.bios.2015.03.049.
(29) Shi, J.; Claussen, J. C.; McLamore, E. S.; Ul Haque, A.; Jaroch, D.; Diggs, A. R.; Calvo-Marzal, P.; Rickus, J. L.; Marshall Porterfield, D. A Comparative Study of Enzyme Immobilization Strategies for Multi-Walled Carbon Nanotube Glucose Biosensors. *Nanotechnology* **2011,** *22* (35), 1-10, DOI: 10.1088/0957-4484/22/35/355502.
(30) Zhu, H.; Li, L.; Zhou, W.; Shao, Z.; Chen, X. Advances in Non-enzymatic Glucose Sensors Based on Metal Oxides. *Journal of Materials Chemistry B* **2016,** *4* (46), 7333-7349, DOI: 10.1039/C6TB02037B.
(31) Luo, Y.; Kong, F.-Y.; Li, C.; Shi, J.-J.; Lv, W.-X.; Wang, W. One-pot Preparation of Reduced Graphene Oxide-Carbon Nanotube Decorated with Au Nanoparticles Based on Protein for Non-enzymatic Electrochemical Sensing of Glucose. *Sensors and Actuators B: Chemical* **2016,** *234*, 625-632, DOI: 10.1016/j.snb.2016.05.046.

(32) Zen, J.-M.; Lo, C.-W. A Glucose Sensor Made of an Enzymatic Clay-Modified Electrode and Methyl Viologen Mediator. *Analytical Chemistry* **1996,** *68* (15), 2635-2640, DOI: 10.1021/ac960090j.
(33) Ghica, M. E.; Brett, C. M. A. A Glucose Biosensor Using Methyl Viologen Redox Mediator on Carbon Film Electrodes. *Analytica Chimica Acta* **2005,** *532* (2), 145-151, DOI: 10.1016/j.aca.2004.10.058.
(34) Watt, G. D. Kinetic Evaluation of the Viologen-Catalyzed Carbohydrate Oxidation Reaction for Fuel Cell Application. *Renewable Energy* **2014,** *63* (Supplement C), 370-375, DOI: 10.1016/j.renene.2013.09.025.
(35) Marr, K. M.; Chen, B.; Mootz, E. J.; Geder, J.; Pruessner, M.; Melde, B. J.; Vanfleet, R. R.; Medintz, I. L.; Iverson, B. D.; Claussen, J. C. High Aspect Ratio Carbon Nanotube Membranes Decorated with Pt Nanoparticle Urchins for Micro Underwater Vehicle Propulsion via H2O2 Decomposition. *ACS Nano* **2015,** *9* (8), 7791-7803, DOI: 10.1021/acsnano.5b02124.
(36) Chen, B.; Garland, N. T.; Geder, J.; Pruessner, M.; Mootz, E.; Cargill, A.; Leners, A.; Vokshi, G.; Davis, J.; Burns, W.; Daniele, M. A.; Kogot, J.; Medintz, I. L.; Claussen, J. C. Platinum Nanoparticle Decorated SiO2 Microfibers as Catalysts for Micro Unmanned Underwater Vehicle Propulsion. *ACS Applied Materials & Interfaces* **2016,** *8* (45), 30941-30947, DOI: 10.1021/acsami.6b10047.
(37) Claussen, J. C.; Daniele, M. A.; Geder, J.; Pruessner, M.; Makinen, A. J.; Melde, B. J.; Twigg, M.; Verbarg, J. M.; Medintz, I. L. Platinum-Paper Micromotors: An Urchin-Like Nanohybrid Catalyst for Green Monopropellant Bubble-Thrusters. *ACS Applied Materials & Interfaces* **2014,** *6* (20), 17837-17847, DOI: 10.1021/am504525e.
(38) Wang, X.; Kim, S. B.; Khang, D.; Kim, H.-H.; Kim, C.-J. Optimization and Characterization of Covalent Immobilization of Glucose Oxidase for Bioelectronic Devices. *Biochemical Engineering Journal* **2016,** *112*, 20-31, DOI: 10.1016/j.bej.2016.03.016.
(39) Bockris, J. O. M.; Oldfield, L. F. The Oxidation-Reduction Reactions of Hydrogen Peroxide at Inert Metal Electrodes and Mercury Cathodes. *Transactions of the Faraday Society* **1955,** *51* (0), 249-259, DOI: 10.1039/TF9555100249.
(40) Anderson, L.; Wittkopp, S. M.; Painter, C. J.; Liegel, J. J.; Schreiner, R.; Bell, J. A.; Shakhashiri, B. Z. What Is Happening When the Blue Bottle Bleaches: An Investigation of the Methylene Blue-Catalyzed Air Oxidation of Glucose. *Journal of Chemical Education* **2012,** *89* (11), 1425-1431, DOI: 10.1021/ed200511d.
(41) De Wit, G.; Kieboom, A. P. G.; van Bekkum, H. Enolisation and Isomerisation of Monosaccharides in Aqueous, Alkaline Solution. *Carbohydrate Research* **1979,** *74* (1), 157-175, DOI: 10.1016/S0008-6215(00)84773-4.
(42) Monk, P. M. S. *The Viologens: Physicochemical Properties, Synthesis and Applications of the Salts of 4,4'-Bipyridine*, Wiley: Chichester, New York, 1998.
(43) Ding, S.; Das, S. R.; Brownlee, B. J.; Parate, K.; Davis, T. M.; Stromberg, L. R.; Chan, E. K. L.; Katz, J.; Iverson, B. D.; Claussen, J. C. CIP2A Immunosensor Comprised of Vertically-aligned Carbon Nanotube Interdigitated Electrodes Towards Point-of-Care Oral Cancer Screening. *Biosensors and Bioelectronics* **2018,** *117*, 68-74, DOI: 10.1016/j.bios.2018.04.016.
(44) Sun, S.; Yang, D.; Zhang, G.; Sacher, E.; Dodelet, J.-P. Synthesis and Characterization of Platinum Nanowire–Carbon Nanotube Heterostructures. *Chemistry of Materials* **2007,** *19* (26), 6376-6378, DOI: 10.1021/cm7022949.

(45) Gonzalez-Gaitan, C.; Ruiz-Rosas, R.; Morallon, E.; Cazorla-Amoros, D. Effects of the Surface Chemistry and Structure of Carbon Nanotubes on the Coating of Glucose Oxidase and Electrochemical Biosensors Performance. *RSC Advances* **2017,** *7* (43), 26867-26878, DOI: 10.1039/C7RA02380D.
(46) Chen, C.; Xie, Q.; Yang, D.; Xiao, H.; Fu, Y.; Tan, Y.; Yao, S. Recent Advances in Electrochemical Glucose Biosensors: A Review. *RSC Advances* **2013,** *3* (14), 4473-4491, DOI: 10.1039/C2RA22351A.

Table of Contents Graphic